

Quantum oscillation signatures of interface Fermi arcs

Adam Yanis Chaou , Vatsal Dwivedi , and Maxim Breitkreiz *

Dahlem Center for Complex Quantum Systems and Fachbereich Physik, Freie Universität Berlin, 14195 Berlin, Germany



(Received 9 November 2023; accepted 13 June 2024; published 8 July 2024)

Fermi-arc surface states of Weyl semimetals exhibit a unique combination of localization to a surface and the connection to the bulk Weyl fermions. We predict characteristic quantum-oscillation signatures of Fermi arcs in the tunnel magnetoelectroconductance across an interface between two Weyl semimetals. These oscillations stem from a momentum-space analog of Aharonov-Bohm interference of electrons moving along the interface Fermi arcs, driven by an external magnetic field normal to the interface. The Fermi arcs' connection to the bulk enables their characterization via transport normal to the interface, while their localization along the transport direction manifests in a strong field-angle anisotropy of the oscillations. This combination distinguishes these oscillations from conventional Shubnikov-de Haas oscillations and makes them identifiable even in the complex oscillation spectra of real materials.

DOI: [10.1103/PhysRevB.110.035116](https://doi.org/10.1103/PhysRevB.110.035116)

I. INTRODUCTION

Weyl semimetals (WSMs) are a class of three-dimensional topological semimetals that host pairs of topologically protected gapless points that can be described as Weyl fermions at low energies [1–11]. A remarkable feature of Weyl fermions is the chiral anomaly [12,13], which can be understood as a spectral flow along the chiral zeroth Landau level dispersing parallel to an applied magnetic field [14]. The boundary manifestation of the bulk topology of WSMs are Fermi arcs—lines of zero-energy surface states that connect projections of opposite-chirality Weyl nodes within the surface Brillouin zone [1,15].

An interface between two WSMs also features Fermi arcs unless Weyl nodes of the same chirality from different WSMs project on top of each other [16–22]. Interface Fermi arcs either connect nodes of opposite chirality from the same WSM (as in the case of surface Fermi arcs), which are termed heterochiral connectivity, or nodes of identical chirality from different WSMs, termed homochiral connectivity. In the presence of a magnetic field normal to the interface (the “longitudinal” direction), charge current carried by the anomalous chiral Landau levels in longitudinal direction is redirected along the Fermi arcs by the Lorentz force. For homochiral Fermi arcs, this leads to perfect transmission of the anomalous charge current [22], while for heterochiral Fermi arcs, it leads to perfect reflection and hence the vanishing of the tunnel conductance. In both cases, the Fermi arcs bear a unique combination of local and nonlocal qualities in that they are localized to the interface but mediate transport normal to it, i.e., along their localization direction [22–24].

Quantum oscillations, such as the Shubnikov-de Haas (SdH) or de Haas-van Alphen effects, constitute standard experimental tools for mapping Fermi surfaces of metals [25].

Identification of Fermi arcs using these well-established techniques has, however, been challenging [26–30]. In principle, Fermi arcs are detectable via quantum oscillations stemming from the so-called Weyl orbit [26,31]—the cyclotron orbit of a thin WSM slab that involves the coherent motion along Fermi arcs on both surfaces of the slab, connected by chiral Landau levels across the slab width. However, in this case the characteristic nonlocality manifests itself only in the slab-width dependence of the oscillation shift, which, alongside the requirement of a small slab width to ensure phase coherence, makes the experimental identification of Fermi arcs very difficult [27,28]. Furthermore, typical WSM materials exhibit additional Fermi pockets, whose trivial orbits also contribute to the full quantum oscillation spectrum.

In this article, we predict a characteristic quantum-oscillation signature of Fermi arcs in the tunnel magnetoelectroconductance. We consider interfaces between two WSMs where Fermi arcs exhibit two or more close encounters, as exemplified in Fig. 1. Such a Fermi-arc configuration can be experimentally realized, e.g., at an interface between two weakly coupled WSMs with curved Fermi arcs. These can be two different WSM materials or two slabs of the same material rotated with respect to each other, such as rotated TaAs (001) surfaces [32,33] shown in Fig. 1(c). We predict oscillations in the magnetoelectroconductance as a function of the inverse longitudinal magnetic-field component, with the oscillation frequency proportional to the momentum-space area enclosed by the Fermi arcs. These originate from the magnetic breakdown at close encounters [34–36] resulting in multiple effective paths [37–39] connecting interface projections of the Weyl nodes, leading to Aharonov-Bohm-like interference in momentum space. The resulting quantum oscillations of the tunnel magnetoelectroconductance are fundamentally different from the possibly coexisting SdH oscillations that stem from Landau-quantized levels passing the Fermi energy. These are experimentally identifiable by a strong field-angle anisotropy—owing to a dependence only on the longitudinal

*Contact author: breitkr@physik.fu-berlin.de

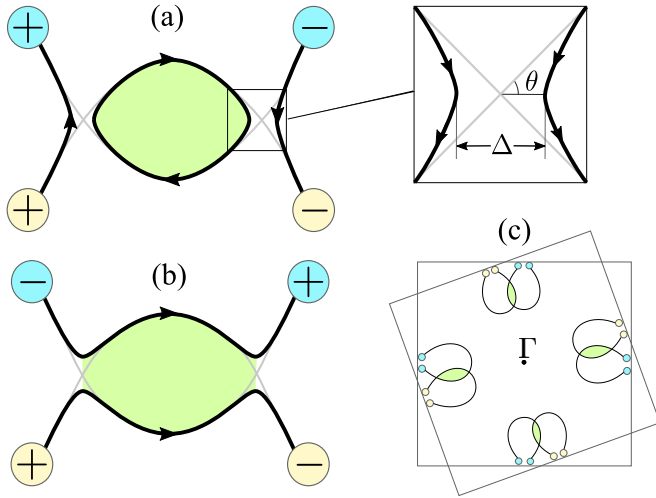


FIG. 1. Fermi-arc configurations (black lines) with (a) homochiral and (b) heterochiral connectivity, exhibiting two close encounters at a weakly coupled interface between two WSMs. The projections of Weyl nodes from the two WSMs are depicted as yellow/blue circles (chirality indicated as $+/-$), the arrows indicate the direction of motion in a magnetic field out of the plane, and the (green) shaded region between the two close encounters determines the frequency of quantum oscillations. The inset shows a single close encounter with the minimum separation Δ and the opening angle 2θ . (c) Long crescent Fermi arcs of two TaAs (001) surfaces from *ab initio* calculations [33] rotated by 20° with respect to each other.

component of the magnetic field and thus a direct consequence of the aforementioned local/nonlocal character of the Fermi arcs—and the characteristic damping of higher harmonics. In the following, we describe the proposed setup, compute the tunnel magnetoconductance semiclassically, and compare the predictions to exact numerical simulations on a lattice model.

II. FERMI-ARC MEDIATED TUNNEL MAGNETOCONDUCTANCE

We consider the tunnel magnetoconductance across an interface between two WSMs, for which at least some of the projections of Weyl nodes onto the interface Brillouin zone do not overlap, such that the interface features Fermi arcs connecting well-separated Weyl-node projections. More precisely, we require this separation to be larger than the inverse magnetic length $\ell_B^{-1} \equiv \sqrt{eB/\hbar}$ ($\sim 0.02 \text{ \AA}^{-1}$ for the maximum realistic magnetic field of $B = 30 \text{ T}$). The interface Fermi arcs result from the hybridization of the surface Fermi arcs of the two WSMs, so that their exact form depends on the specific Fermi-arc arrangements of the two coupled surfaces and the coupling strength. If the surface Fermi arcs from the two sides intersect, then a weak coupling generally leads to an avoided crossing in momentum space [see Figs. 1(a) and 1(b)], which we term a “close encounter.”

A pair of interface Fermi arcs contributes the tunnel conductance [22]

$$G = \frac{e^2}{h} N_B T, \quad (1)$$

where e^2/h is the quantum of conductance, $N_B \propto B$ is the Landau level degeneracy (number of flux quanta through the interface), and $0 < T < 1$ is the total transmission probability along the Fermi arcs. For a pair of homochiral (heterochiral) Fermi arcs that are well separated everywhere (i.e., for separations $\gg \ell_B^{-1}$), the transmission probability is $T = 1$ ($T = 0$). In the former case, this implies a universal conductance independent of band details such as Fermi-arc shape, Fermi velocity, and Fermi energy. However, if two Fermi arcs approach within $\sim \ell_B^{-1}$, then magnetic breakdown leads to suppression (enhancement) of the transmission probability for the homochiral (heterochiral) Fermi arcs. In particular, for large fields, this results in $T \propto 1/B$, leading to the saturation of the conductance [22]. Unlike the contributions of trivial states to the magnetoconductance, the Fermi-arc contribution does not show SdH quantum oscillations because the Fermi-arc mediated current is carried exclusively by the lowest Landau levels of Weyl Fermions at all field strengths [40].

We now show that anomalous, non-SdH quantum oscillations occur for Fermi-arc arrangements with more than one close encounter. In case of two encounters, the two possible interface Fermi arc configurations are depicted in Figs. 1(a) and 1(b), which exhibit homochiral and heterochiral connectivity, respectively. In the absence of magnetic breakdown, these two configurations would yield $G = (e^2/h)N_B$ and $G = 0$, respectively (in analogy with the single-encounter case [22]). We next compute the transmission probability in the presence of magnetic breakdown. For simplicity, we focus on the two scenarios depicted in Figs. 1(a) and 1(b) but our analysis can be straightforwardly extended to more nodes and/or more encounters.

III. SEMICLASSICAL ANALYSIS

To compute the transmission amplitudes, we employ a semiclassical approach away from the close encounters coupled with the full quantum problem near them. Semiclassically, the electron wavepackets incident on the interface at a Weyl-node projection are driven along the Fermi arc by the Lorentz force until they are absorbed by another Weyl node of identical/opposite chirality, leading to transmission/reflection across the interface. The quantum effects are encoded in the path-dependent Aharonov-Bohm, de Broglie, and Maslov phases picked up by them [41]. Near a close encounter, the description of magnetic breakdown maps onto the Landau-Zener problem [36,42]. Thus, the splitting of electron trajectories is described by the S-matrix [36]

$$S(B) = \begin{pmatrix} \sqrt{1 - e^{-\gamma}} e^{i\alpha} & -i\sqrt{e^{-\gamma}} \\ -i\sqrt{e^{-\gamma}} & \sqrt{1 - e^{-\gamma}} e^{-i\alpha} \end{pmatrix}, \quad (2)$$

where $\gamma = B_0/B$, $e^{-\gamma}$ is the tunneling probability, and

$$\alpha = \frac{\pi}{4} + \frac{\gamma}{2\pi} \left[1 - \ln \left(\frac{\gamma}{2\pi} \right) \right] + \arg \Gamma \left(\frac{i\gamma}{2\pi} \right) \quad (3)$$

is the additional phase acquired by a state when it does not tunnel. The scattering process is governed by a single free parameter, the breakdown field B_0 , which is determined by

the geometry of the close encounter as

$$B_0 = \frac{\pi}{4} \Delta^2 \tan \theta, \quad (4)$$

where θ is the angle of intersection between the two Fermi arcs in the decoupled limit and Δ is the minimum separation [see inset of Fig. 1(a)]. The total transmission amplitude is the sum over all paths weighted with the scattering amplitudes of the encounters given in (2) and phase factors stemming from motion along the connecting Fermi-arc segments.

For the heterochiral Fermi-arc configuration with two identical encounters depicted in Fig. 1(b) (see the Supplemental Material (SM) [43] for a detailed derivation), the sum over two possible paths leads to the transmission probability

$$T_{\text{het}} = 2e^{-\gamma}(1 - e^{-\gamma})[1 + \cos(\beta - 2\alpha)], \quad (5)$$

where

$$\beta = \frac{\mathcal{A}}{B} + \pi. \quad (6)$$

Here, β is the difference between the de Broglie and Aharonov-Bohm phases acquired along the two paths between the close encounters, given by the momentum space area \mathcal{A} enclosed by the Fermi arcs between the two points of minimum separation at the Fermi level. The additional π in β is a Maslov phase [41] corresponding to the two classical turning points encountered in going around the loop. The magnetoconductance oscillates as a function of B^{-1} , with a slowly varying envelope given by $T_{\text{het}}^{\text{max}} = 4e^{-\gamma}(1 - e^{-\gamma})$. For $B \rightarrow 0$, we get an exponentially suppressed $T_{\text{het}} \simeq 4e^{-\gamma}$, vanishing as expected for interface Fermi arcs connecting the nodes from the same WSM. For $B \rightarrow \infty$, $T_{\text{het}}^{\text{max}} \approx 4B_0/B$, so that the conductance saturates at a value proportional to B_0 .

For the homochiral configuration [Fig. 1(a)], there are infinitely many paths leading to transmission, corresponding to tunneling into the loop of zero modes, traversing it arbitrarily many times, and finally tunneling out of it on the same side of the loop. Summing over these possibilities, we obtain the transmission probability as

$$T_{\text{hom}} = 1 - \frac{e^{-2\gamma}}{e^{-2\gamma} + 2(1 - e^{-\gamma})[1 - \cos(\beta + 2\alpha)]}, \quad (7)$$

where β is again given by Eq. (6). The difference in the sign of α originates from the opposite signs of the Landau-Zener phases acquired by the two Fermi arcs involved in a close encounter. The magnetoconductance also oscillates as a function of B^{-1} , with the envelope given by $T_{\text{hom}}^{\text{max}} = 4(1 - e^{-\gamma})/(2 - e^{-\gamma})^2$. For $B \rightarrow 0$, we get $T_{\text{hom}} = 1$ as expected for homochiral Fermi arcs, leading to a linear-in- B magnetoconductance. The limit $B \rightarrow \infty$ again leads to saturation of the magnetoconductance $T_{\text{hom}}^{\text{max}} \approx 4B_0/B$.

In Fig. 2, we plot the conductance [given by Eq. (1)] as well as the tunnel probability and its Fourier transform for a specific value of parameters and compare them with numerical simulations on a lattice model (detailed below). While the conductance shows qualitatively similar features for both homochiral and heterochiral connectivities [44], they can be easily distinguished by the Fourier transform. For the heterochiral connectivity, as the oscillations result from the interference of only two paths, the Fourier transform exhibits a single peak, with the frequency corresponding to

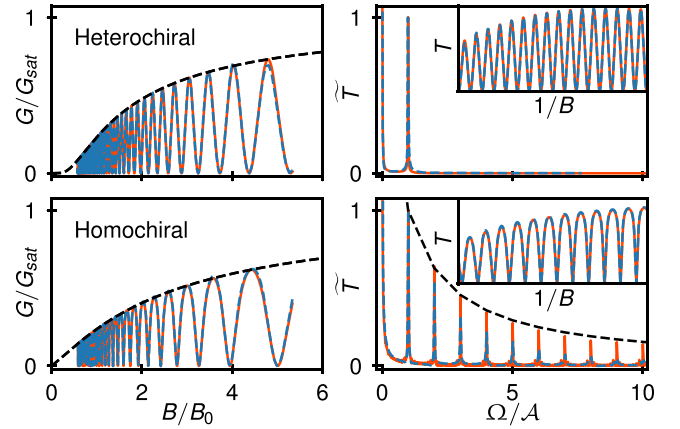


FIG. 2. Left column: Conductance as a function of magnetic field for heterochiral (top row) and homochiral (bottom row) connectivity obtained from analytics (solid orange lines) and numerics (dashed blue lines). Right: Fourier transform of tunnel probability $\tilde{T}(\Omega)$ normalized to $\tilde{T}(\mathcal{A}) = 1$ [inset shows $T(1/B)$]. The dashed black line shows the analytically obtained damping of higher harmonics. Model parameters are $\kappa = 0.07$ and $\varepsilon_F = 0.1$ (others in text).

the area \mathcal{A} enclosed between the two Fermi arcs. On the other hand, for homochiral connectivities, the trivial loop connecting the homochiral Fermi arcs can be traversed multiple times (similar to SdH oscillations), leading to harmonics at frequencies $n\mathcal{A}$. In contrast to SdH oscillations, however, for each traversal of the loop, there is a nonzero probability of tunneling out of the loop to the opposite Fermi arc, leading to reflection from the interface. Thus, the higher harmonics are damped, with the height of the n th peak proportional to $[\Psi(n/2 + 1) - \Psi(n/2 + 1/2)]$, where $\Psi(z) = \Gamma'(z)/\Gamma(z)$ is the digamma function (see the SM [43] for the derivation). This damping profile exhibits a long tail and should be visible even for small \mathcal{A} .

In our analysis, we assumed that the two encounters are identical; the qualitative behavior of the quantum oscillations is unchanged for the case of two different encounters, as we show in the SM [43]. The lower envelope of oscillations will deviate from zero in this case, as the destructive interference of the now differently weighted paths will no longer lead to perfect cancellation.

IV. LATTICE MODEL AND NUMERICAL RESULTS

We compare our analytical predictions with a numerical simulation on an explicit lattice model, for which we compute the model-specific parameters Δ , θ , and \mathcal{A} that enter the analytical formula, so that analytics and numerics can be compared without any fitting parameters. We consider a Bloch Hamiltonian of the form [45]

$$\mathcal{H}(\mathbf{k}) = \mathcal{H}_x(k_x) + \eta_y(\mathbf{k}_\perp)\tau^y + \eta_z(\mathbf{k}_\perp)\tau^z, \quad (8)$$

where the Pauli matrices τ^a represent a pseudospin degree of freedom and

$$\mathcal{H}_x(k_x) = \sin k_x \tau^x + (1 - \cos k_x) \tau^z. \quad (9)$$

The lattice constant and the hopping strength along x are set to unity. This lattice model has Weyl nodes in the $k_x = 0$ plane

at transverse momenta \mathbf{k}_\perp that satisfy $\eta_y(\mathbf{k}_\perp) = \eta_z(\mathbf{k}_\perp) = 0$. For a surface normal to x , the Fermi arcs are given by [45] $\eta_y(\mathbf{k}_\perp) = 0$, which exist only for lattice momenta satisfying $\eta_z(\mathbf{k}_\perp) < 0$.

We consider an interface between two WSMs that are described by the lattice model above with

$$\begin{aligned}\eta_y^A(\mathbf{k}_\perp) &= \xi_A(\cos k_y - \cos b_y + \zeta_A \sin k_z - \sin b_z), \\ \eta_z^A(\mathbf{k}_\perp) &= \cos b_z - \cos k_z,\end{aligned}\quad (10)$$

where $A \in \{\text{L}, \text{R}\}$, $b_y, b_z \in (0, \pi)$, and $\xi_A, \zeta_A \in \{\pm 1\}$. The two WSMs have Weyl nodes at $\mathbf{k}_A = (0, \pm b_y, \zeta_A b_z)$ with chiralities $\chi = \pm \xi_A \zeta_A$. We model the tunnel junction by modulating the hopping along x at the interface by a factor $0 \leq \kappa \leq 1$. To ensure that in the decoupled limit ($\kappa = 0$), the Fermi arcs of the two sides intersect at two points, we set $\zeta_L = -\zeta_R = -1$. The intersection point is then given by $\mathbf{k}_\perp = (\pm b_0, 0)$ with $b_0 \equiv \cos^{-1}(\cos b_y + \sin b_z)$. For $\kappa > 0$, the Fermi arc connectivity is homochiral if $\xi_L = -\xi_R = 1$ and heterochiral if $\xi_L = \xi_R = 1$. We hereafter set $b_y = 3\pi/4$ and $b_z = \pi/2$ so that $b_0 = \cos^{-1}(1 - 2^{-1/2}) \approx 0.4\pi$.

We obtain θ by linearizing the Fermi arc contours $\eta_y^{L/R}(\mathbf{k}_\perp) = 0$ about the intersection points $(\pm b_0, 0)$. This yields $q_z \approx -\zeta_{L/R} \sin b_0 q_y$, so that θ is given by $\tan \theta = |q_z/q_y| = |\sin b_0|$ ($\tan \theta = |q_y/q_z| = |\csc b_0|$) for homochiral (heterochiral) connectivity. To compute Δ and \mathcal{A} , we employ generalized transfer matrices [45,46] as detailed in the SM [43]. This yields an implicit expression for the interface Fermi arcs in terms of ε , \mathbf{k}_\perp , and κ . Using the fact that the minimum separation $\Delta(\kappa)$ occurs along the lines $k_z = 0$ and $k_y = \pm b_0$ for the homochiral and heterochiral cases, respectively, we obtain

$$\begin{aligned}\Delta_{\text{hom}}(\kappa) &= \cos^{-1}(\cos b_0 - \kappa) - \cos^{-1}(\cos b_0 + \kappa) \\ &\approx 2\kappa \csc b_0 + \mathcal{O}(\kappa^3),\end{aligned}\quad (11)$$

and

$$\begin{aligned}\Delta_{\text{het}}(\kappa) &= 2 \left[\cos^{-1} \left(\frac{\kappa}{1 + \kappa^2} \right) - \tan^{-1} \left(\frac{1 - \kappa^2}{2\kappa} \right) \right] \\ &\approx 2\kappa + \mathcal{O}(\kappa^3).\end{aligned}\quad (12)$$

The computation of \mathcal{A} is analytically intractable, so that we obtain it by numerically integrating the implicit condition for the Fermi arcs at $\varepsilon = \varepsilon_F$. Inserting the expressions for Δ and $\tan \theta$ into Eq. (4), we obtain the breakdown field which, together with \mathcal{A} , determines the analytic magnetoconductance via Eqs. (5) and (7) inserted into (1). The exact numerical computation of the magnetoconductance is performed using the Kwant package [47]. We find perfect agreement between the analytics and numerics without any fitting parameter, as exemplified in Fig. 2, for the relevant range of parameters κ , ε_F , and B , set by the requirement $\mathcal{A} \gtrsim l_B^{-2} \sim l_{B_0}^{-2}$ to ensure observable oscillations (not

too small oscillation frequencies) and uncoupled Weyl-node projections.

V. DISCUSSION AND CONCLUSIONS

We have demonstrated anomalous quantum oscillations in the tunnel magnetoconductance across a Weyl semimetal interface, arising from a momentum-space Aharonov-Bohm interference, enabled by magnetic breakdown in Fermi-arc networks. As the oscillations appear in the electron transport normal to the interface, and thus along the Fermi-arc localization direction, they exemplify the unique combination of local and nonlocal qualities of Fermi arcs.

An experimental fingerprint of the anomalous oscillations is a field-angle anisotropy: since the Fermi-arc contributions only depend on the longitudinal field component, the oscillation frequency is proportional to $1/\cos \theta$, with θ being the angle between the the magnetic field and the current. This distinguishes them from other quantum oscillations that may arise from various two- or three-dimensional trivial Fermi pockets. The former do not contribute to transport along their localization direction, while the latter do not have a frequency proportional to $1/\cos \theta$, which is characteristic for two-dimensional Fermi surfaces. This Fermi-arc signature should thus be better accessible than the width dependence of SdH oscillation shifts of Weyl orbits.

Further peculiarities lie in the behavior of higher harmonics of the anomalous oscillations, which, moreover, allow to distinguish different Fermi-arc connectivities. For heterochiral connectivity, the spectrum does not feature higher harmonics (unlike the SdH oscillations), while for homochiral connectivity, the higher harmonics feature unusual damping stemming from magnetic breakdown.

As the Fermi arc contribution to quantum oscillations requires coherent transport along the full loop of interface states, we expect them to be sensitive to temperature and disorder-induced decoherence, similar to conventional SdH oscillations [25]. The real-space distance traversed by the electron while completing n loops of length K is $nl_B^2 K$. For $K \sim 1 \text{ nm}^{-1}$ [the order of the loop for the TaAs twisted surfaces in Fig. 1(c)] this gives a coherence length of $\sim n \times 700 \text{ nm}/B[\text{T}]$ for the observation of the n th harmonic, which makes an observation of the first few harmonics realistic for available sample qualities and field strengths [48]. These constraints on coherence are less stringent than those required for the observation of Weyl orbits, making the anomalous quantum oscillations a more suitable probe for investigating Fermi arc connectivities.

ACKNOWLEDGMENTS

We thank P. W. Brouwer, L. I. Glazman, M. Mansouri, S. A. Parameswaran, and S. Wiedmann for useful discussions. This research was funded by the Deutsche Forschungsgemeinschaft (DFG, German Research Foundation), Project Grant No. 277101999, through CRC-TR 183 (sub-projects A02 and A03) ‘‘Entangled States of Matter’’ and the Emmy Noether program, Project No. 506208038.

- [1] X. Wan, A. M. Turner, A. Vishwanath, and S. Y. Savrasov, Topological semimetal and Fermi-arc surface states in the electronic structure of pyrochlore iridates, *Phys. Rev. B* **83**, 205101 (2011).
- [2] A. A. Burkov and L. Balents, Weyl semimetal in a topological insulator multilayer, *Phys. Rev. Lett.* **107**, 127205 (2011).
- [3] G. Xu, H. Weng, Z. Wang, X. Dai, and Z. Fang, Chern semimetal and the quantized anomalous Hall effect in HgCr_2Se_4 , *Phys. Rev. Lett.* **107**, 186806 (2011).
- [4] S.-Y. Xu, C. Liu, S. K. Kushwaha, R. Sankar, J. W. Krizan, I. Belopolski, M. Neupane, G. Bian, N. Alidoust, T.-R. Chang, H.-T. Jeng, C.-Y. Huang, W.-F. Tsai, H. Lin, P. P. Shibayev, F.-C. Chou, R. J. Cava, and M. Z. Hasan, Observation of Fermi arc surface states in a topological metal, *Science* **347**, 294 (2015).
- [5] S.-Y. Xu, N. Alidoust, I. Belopolski, Z. Yuan, G. Bian, T.-R. Chang, H. Zheng, V. N. Strocov, D. S. Sanchez, G. Chang, C. Zhang, D. Mou, Y. Wu, L. Huang, C.-C. Lee, S.-M. Huang, B. Wang, A. Bansil, H.-T. Jeng, T. Neupert, A. Kaminski, H. Lin, S. Jia, and M. Z. Hasan, Discovery of a Weyl fermion state with Fermi arcs in niobium arsenide, *Nat. Phys.* **11**, 748 (2015).
- [6] B. Q. Lv, H. M. Weng, B. B. Fu, X. P. Wang, H. Miao, J. Ma, P. Richard, X. C. Huang, L. X. Zhao, G. F. Chen, Z. Fang, X. Dai, T. Qian, and H. Ding, Experimental discovery of Weyl semimetal TaAs, *Phys. Rev. X* **5**, 031013 (2015).
- [7] N. P. Armitage, E. J. Mele, and A. Vishwanath, Weyl and Dirac semimetals in three dimensional solids, *Rev. Mod. Phys.* **90**, 015001 (2018).
- [8] B. Yan and C. Felser, Topological materials: Weyl semimetals, *Annu. Rev. Condens. Matter Phys.* **8**, 337 (2017).
- [9] A. A. Burkov, Weyl metals, *Annu. Rev. Condens. Matter Phys.* **9**, 359 (2018).
- [10] M. Z. Hasan, G. Chang, I. Belopolski, G. Bian, S. Y. Xu, and J. X. Yin, Weyl, Dirac and high-fold chiral fermions in topological quantum matter, *Nat. Rev. Mater.* **6**, 784 (2021).
- [11] B. A. Bernevig, C. Felser, and H. Beidenkopf, Progress and prospects in magnetic topological materials, *Nature (London)* **603**, 41 (2022).
- [12] S. L. Adler, Axial-vector vertex in spinor electrodynamics, *Phys. Rev.* **177**, 2426 (1969).
- [13] J. S. Bell and R. W. Jackiw, A PCAC puzzle: $\pi^0 \rightarrow \gamma\gamma$ in the σ -model, *Nuovo Cim. A* **60**, 47 (1969).
- [14] H. B. Nielsen and M. Ninomiya, The Adler-Bell-Jackiw anomaly and Weyl fermions in a crystal, *Phys. Lett. B* **130**, 389 (1983).
- [15] N. Morali, R. Batabyal, P. K. Nag, E. Liu, Q. Xu, Y. Sun, B. Yan, C. Felser, N. Avraham, and H. Beidenkopf, Fermi-arc diversity on surface terminations of the magnetic Weyl semimetal $\text{Co}_3\text{Sn}_2\text{S}_2$, *Science* **365**, 1286 (2019).
- [16] V. Dwivedi, Fermi arc reconstruction at junctions between Weyl semimetals, *Phys. Rev. B* **97**, 064201 (2018).
- [17] F. Abdulla, S. Rao, and G. Murthy, Fermi arc reconstruction at the interface of twisted Weyl semimetals, *Phys. Rev. B* **103**, 235308 (2021).
- [18] N. Mathur, F. Yuan, G. Cheng, S. Kaushik, I. Robredo, and G. Maia, Atomically sharp internal interface in a chiral Weyl semimetal nanowire, *Nano Lett.* **23**, 2695 (2023).
- [19] S. Kaushik, I. Robredo, N. Mathur, L. M. Schoop, S. Jin, M. G. Vergniory, and J. Cano, Transport signatures of Fermi arcs at twin boundaries in Weyl materials, [arXiv:2207.14109](https://arxiv.org/abs/2207.14109).
- [20] G. Murthy, H. A. Fertig, and E. Shimshoni, Surface states and arcless angles in twisted Weyl semimetals, *Phys. Rev. Res.* **2**, 013367 (2020).
- [21] R. Kundu, H. A. Fertig, and A. Kundu, Broken symmetry and competing orders in Weyl semimetal interfaces, *Phys. Rev. B* **107**, L041402 (2023).
- [22] A. Y. Chaou, V. Dwivedi, and M. Breikreuz, Magnetic breakdown and chiral magnetic effect at Weyl-semimetal tunnel junctions, *Phys. Rev. B* **107**, L241109 (2023).
- [23] S. A. Parameswaran, T. Grover, D. A. Abanin, D. A. Pesin, and A. Vishwanath, Probing the chiral anomaly with nonlocal transport in three-dimensional topological semimetals, *Phys. Rev. X* **4**, 031035 (2014).
- [24] Y. Baum, E. Berg, S. A. Parameswaran, and A. Stern, Current at a distance and resonant transparency in Weyl semimetals, *Phys. Rev. X* **5**, 041046 (2015).
- [25] D. Shoenberg, *Magnetic Oscillations in Metals*, Cambridge Monographs on Physics (Cambridge University Press, Cambridge, 1984).
- [26] P. J. W. Moll, N. L. Nair, T. Helm, A. C. Potter, I. Kimchi, A. Vishwanath, and J. G. Analytis, Transport evidence for Fermi-arc-mediated chirality transfer in the Dirac semimetal Cd_3As_2 , *Nature (London)* **535**, 266 (2016).
- [27] L. Galletti, T. Schumann, D. A. Kealhofer, M. Goyal, and S. Stemmer, Absence of signatures of Weyl orbits in the thickness dependence of quantum transport in cadmium arsenide, *Phys. Rev. B* **99**, 201401(R) (2019).
- [28] U. Kar, A. K. Singh, Y.-T. Hsu, C.-Y. Lin, B. Das, C.-T. Cheng, M. Berben, S. Yang, C.-Y. Lin, C.-H. Hsu, S. Wiedmann, W.-C. Lee, and W.-L. Lee, The thickness dependence of quantum oscillations in ferromagnetic Weyl metal SrRuO_3 , *npj Quantum Mater.* **8**, 8 (2023).
- [29] N. L. Nair, M. E. Boulanger, F. Laliberté, S. Griffin, S. Channa, A. Legros, W. Tabis, C. Proust, J. Neaton, L. Taillefer, and J. G. Analytis, Signatures of possible surface states in TaAs, *Phys. Rev. B* **102**, 075402 (2020).
- [30] C. Zhang, Z. Ni, J. Zhang, X. Yuan, Y. Liu, Y. Zou, Z. Liao, Y. Du, A. Narayan, H. Zhang, T. Gu, X. Zhu, L. Pi, S. Sanvito, X. Han, J. Zou, Y. Shi, X. Wan, S. Y. Savrasov, and F. Xiu, Ultrahigh conductivity in Weyl semimetal NbAs nanobelts, *Nat. Mater.* **18**, 482 (2019).
- [31] A. Potter, I. Kimchi, and A. Vishwanath, Quantum oscillations from surface Fermi-arcs in Weyl and Dirac semi-metals, *Nat. Commun.* **5**, 5161 (2014).
- [32] S.-Y. Xu, N. Alidoust, I. Belopolski, Z. Yuan, G. Bian, T.-R. Chang, H. Zheng, V. N. Strocov, D. S. Sanchez, G. Chang, C. Zhang, D. Mou, Y. Wu, L. Huang, C.-C. Lee, S.-M. Huang, B. Wang, A. Bansil, H.-T. Jeng, T. Neupert, A. Kaminski, H. Lin, S. Jia, and M. Zahid Hasan, Discovery of a Weyl fermion semimetal and topological Fermi arcs, *Science* **349**, 613 (2015).
- [33] G. Chang, S.-Y. Xu, H. Zheng, C.-C. Lee, S.-M. Huang, I. Belopolski, D. S. Sanchez, G. Bian, N. Alidoust, T.-R. Chang, C.-H. Hsu, H.-T. Jeng, A. Bansil, H. Lin, and M. Z. Hasan, Signatures of Fermi arcs in the quasiparticle interferences of the Weyl semimetals TaAs and NbP, *Phys. Rev. Lett.* **116**, 066601 (2016).

- [34] M. H. Cohen and L. M. Falicov, Magnetic breakdown in crystals, *Phys. Rev. Lett.* **7**, 231 (1961).
- [35] E. I. Blount, Bloch electrons in a magnetic field, *Phys. Rev.* **126**, 1636 (1962).
- [36] M. I. Kaganov and A. A. Slutskin, Coherent magnetic breakdown, *Phys. Rep.* **98**, 189 (1983).
- [37] L. M. Falicov and H. Stachowiak, Theory of the de Haas-van Alphen effect in a system of coupled orbits. Application to magnesium, *Phys. Rev.* **147**, 505 (1966).
- [38] M. R. van Delft, S. Pezzini, T. Khouri, C. S. A. Mueller, M. Breitzkreiz, L. M. Schoop, A. Carrington, N. E. Hussey, and S. Wiedmann, Electron-hole tunneling revealed by quantum oscillations in the nodal-line semimetal HfSiS, *Phys. Rev. Lett.* **121**, 256602 (2018).
- [39] C. S. Müller, T. Khouri, M. R. van Delft, S. Pezzini, Y. T. Hsu, J. Ayres, M. Breitzkreiz, L. M. Schoop, A. Carrington, N. E. Hussey, and S. Wiedmann, Determination of the Fermi surface and field-induced quasi-particle tunneling around the Dirac nodal-loop in ZrSiS, *Phys. Rev. Res.* **2**, 023217 (2020).
- [40] M. Breitzkreiz and P. W. Brouwer, Fermi-arc metals, *Phys. Rev. Lett.* **130**, 196602 (2023).
- [41] J. B. Keller, Corrected Bohr-Sommerfeld quantum conditions for nonseparable systems, *Ann. Phys.* **4**, 180 (1958).
- [42] L. D. Landau and E. M. Lifshitz, *Quantum Mechanics: Non-Relativistic Theory*, Course of Theoretical Physics Vol. 3 (Pergamon Press, Oxford, 1977).
- [43] See Supplemental Material at <http://link.aps.org/supplemental/10.1103/PhysRevB.110.035116> for the derivation of the S-matrix for the two interface Fermi arc connectivities and the derivation of various parameters from the lattice model.
- [44] The low- B behavior are different for the two cases due to the different transmissions for $B \ll B_0$ but we are here interested in the regime of observable oscillations, which is $B \sim B_0$.
- [45] V. Dwivedi and V. Chua, Of bulk and boundaries: Generalized transfer matrices for tight-binding models, *Phys. Rev. B* **93**, 134304 (2016).
- [46] V. Dwivedi and S. T. Ramamurthy, Connecting the dots: Time-reversal symmetric Weyl semimetals with tunable Fermi arcs, *Phys. Rev. B* **94**, 245143 (2016).
- [47] C. W. Groth, M. Wimmer, A. R. Akhmerov, and X. Waintal, Kwant: a software package for quantum transport, *New J. Phys.* **16**, 063065 (2014).
- [48] F. Arnold, M. Naumann, S. C. Wu, Y. Sun, M. Schmidt, H. Borrmann, C. Felser, B. Yan, and E. Hassinger, Chiral Weyl pockets and Fermi surface topology of the Weyl semimetal TaAs, *Phys. Rev. Lett.* **117**, 146401 (2016).